Cellular FLIP Protects KSHV-Transformed Lymphoma Cells from TRAIL-Independent TRAIL Receptor 1-Mediated Cell Death

Neil Kuehnle[1], Mark Manzano[2], Eva Gottwein[1]

*Corresponding author, email: e-gottwein@northwestern.edu; phone: 312-503-3075

[1]Department of Microbiology-Immunology, Northwestern University, Feinberg School of Medicine, Tarry 6-735, Chicago, Illinois, 60611, USA

[2]Current Address: Mark Manzano, Department of Microbiology and Immunology, University of Arkansas for Medical Sciences, Little Rock, Arkansas, USA.

Abstract

Kaposi's sarcoma-associated herpesvirus (KSHV) causes primary effusion lymphoma (PEL). PEL cell lines require expression of the cellular FLICE inhibitory protein (cFLIP) for survival, although KSHV encodes a viral homolog of this protein (vFLIP). Cellular and viral FLIP proteins have several functions, including, most importantly, the inhibition of pro-apoptotic caspase 8 and modulation of NF-κB signaling. To investigate the essential role of cFLIP and its potential redundancy with vFLIP in PEL cells, we first performed rescue experiments with human or viral FLIP proteins known to affect FLIP target pathways differently. The long and short isoforms of cFLIP and molluscum contagiosum virus MC159L, which are all strong caspase 8 inhibitors, efficiently rescued the loss of endogenous cFLIP activity in PEL cells. KSHV vFLIP was unable to fully rescue the loss of endogenous cFLIP and is therefore functionally distinct. Next, we

employed genome-wide CRISPR/Cas9 synthetic rescue screens to identify loss of function perturbations that can compensate for cFLIP knockout. Results from these screens and our validation experiments implicate the canonical cFLIP target caspase 8 and TRAIL receptor 1 (TRAIL-R1 or TNFRSF10A) in promoting constitutive death signaling in PEL cells. However, this process was independent of TRAIL receptor 2 or TRAIL, the latter of which is not detectable in PEL cell cultures. The requirement for cFLIP is also overcome by inactivation of the ER/Golgi resident chondroitin sulfate proteoglycan synthesis and UFMylation pathways, Jagunal homolog 1 (JAGN1) or CXCR4. UFMylation and JAGN1, but not chondroitin sulfate proteoglycan synthesis or CXCR4, contribute to TRAIL-R1 expression. In sum, our work shows that cFLIP is required in PEL cells to inhibit ligand-independent TRAIL-R1 cell death signaling downstream of a complex set of ER/Golgi-associated processes that have not previously been implicated in cFLIP or TRAIL-R1 function.

Introduction

Primary effusion lymphoma (PEL) is a non-Hodgkin lymphoma comprised of KSHV-transformed B cells that typically accumulate in body cavities[1, 2]. PEL is primarily seen in HIV/AIDS patients and has a poor prognosis, with an average survival below two years[3]. Although the etiology of PEL is incompletely understood, latently expressed KSHV oncoproteins are thought to play essential roles in the KSHV-mediated transformation of PEL cells, including the latency-associated nuclear antigen (LANA), viral interferon regulatory factor 3 (vIRF3), a KSHV-encoded D type cyclin (vCyc), and viral FLICE-inhibitory protein (vFLIP). Indeed, cultured patient derived PEL cell lines depend on the continued expression of several latency genes [4, 5]. vFLIP is considered a major candidate for a viral driver of KSHV-mediated B cell transformation in PEL due to its well-documented ability to activate NF-κB survival signaling [6]. A previous study by our lab explored the dependency of PEL cell lines on cellular genes using genome-wide

49 CRISPR knockout screens [7]. This study identified a surprising dependency on cellular FLIP
50 (cFLIP, encoded by *CFLAR*), despite the presence of the KSHV-encoded vFLIP locus. This
51 study furthermore showed that only two of eight tested PEL cell lines depended on genes
52 related to NF-κB signaling. These unexpected findings prompted us to further investigate the
53 role of cFLIP in the context of KSHV-transformed PEL cell lines and to differentiate it from that
54 of vFLIP.

55 Canonically, FLIP proteins act as dominant-negative inhibitors of caspase 8 (*CASP8*)-
56 induced apoptosis by preventing formation of the death-inducing signaling complex (DISC) or
57 directly inhibiting active CASP8[8, 9, 10, 11]. Non-canonical cFLIP activities have been identified,
58 including the regulation of NF-κB signaling[6, 12]. While KSHV vFLIP is a strong activator of NF-κB
59 signaling, it is currently unclear whether vFLIP is a potent inhibitor of CASP8 [13, 14, 15]. CASP8 is a
60 pro-apoptotic protein in the cysteine protease (caspase) family that typically acts as the initiator
61 caspase in the extrinsic apoptotic pathway induced by the death ligands tumor necrosis factor α
62 (TNFα), Fas ligand, or TNF-related apoptosis-inducing ligand (TRAIL) (as reviewed in [16]). The
63 binding of these ligands to their specific death receptors initiates the formation of the death-
64 inducing signaling complex (DISC), containing Fas-associated death domain (FADD) protein
65 and inactive pro-CASP8. Autocatalytic cleavage of pro-CASP8 in DISC generates active
66 CASP8, which initiates apoptosis. However, additional cellular processes converge on CASP8
67 to regulate cell death, including necroptosis, pyroptosis, autophagy-dependent cell death, and
68 hyperactivation of the ER stress pathway/the unfolded protein response (UPR) [17, 18, 19, 20, 21, 22].

69 Here, we sought to clarify the respective roles of cFLIP and vFLIP in PEL. Our results
70 show that vFLIP is robustly expressed only in a subset of PEL cell lines, which also depend on
71 genes that function in NF-κB signaling. The tight correlation of vFLIP expression with NF-κB
72 dependency in PEL cell lines suggests that vFLIP functions in its well-established role as an
73 activator of the NF-κB pathway in PEL. vFLIP cannot fully compensate for the absence of

74 cFLIP, pointing to a non-redundant function of cFLIP in PEL cells. Using genetic screening and
75 validation experiments, we established that cFLIP is required to inhibit ligand-independent
76 constitutive death signaling by one of the TRAIL receptors, TRAIL-R1 (encoded by
77 *TNFRSF10A*).

78

79 **Results**

80 **vFLIP expression is variable in PEL cell lines**

81 We first examined the expression of human cFLIP and cyclin D2 and their viral homologs vFLIP
82 and vCyc across 8 PEL cell lines and the KSHV-negative B cell line BJAB. As a control, we
83 analyzed KSHV vIRF3, which is latently expressed in PEL from a distinct KSHV locus[4]. We
84 observed comparable expression of the major isoforms of cFLIP, cyclin D2, and KSHV vIRF3
85 across the PEL cell lines (Fig. 1A); In contrast, vFLIP and vCyc expression varied greatly, with
86 vFLIP expression detected only in BC-1 and BC-3. Importantly, these are the same two PEL cell
87 lines shown to depend on NF-κB signaling genes in our previous study of cellular gene
88 dependency in PEL cells (Fig. 1A, bottom)[7]. vCyc expression mirrored the expression of vFLIP,
89 as expected due to their bicistronic expression[23], with the surprising exception of BC-2. Serial
90 dilution of BC-3 lysates suggested that our Western protocol is sensitive enough to detect vFLIP
91 and vCyc expression levels that are ~20-50 fold below those of BC-3 (Fig. S1A, B). The
92 observed patterns of vFLIP expression and NF-κB dependency are consistent with the
93 published role of vFLIP in the activation of NF-κB survival signaling [6, 15, 24, 25, 26, 27], in the subset
94 of PEL cell lines where vFLIP is expressed.

95 **cFLIP is broadly essential in PEL cell lines**

96 We previously validated cFLIP dependency of the PEL cell line BCBL-1[7]. To establish cFLIP
97 dependency more broadly across PEL cell lines, we performed single guide RNA (sgRNA)-

98 induced functional inactivation (KO) of cFLIP followed by cumulative growth curve analysis
99 relative to an sgRNA that targets a safe harbor locus (sgAAVS1) in BCBL-1/Cas9 and 4
100 additional Cas9-expressing PEL cell lines (Fig. 1B, Fig. S1C). The cFLIP sgRNAs lack
101 homology to vFLIP and did not affect vFLIP expression in BC-3 cells (Fig. S1D). For BC-1,
102 which did not show significant depletion of cFLIP-specific sgRNAs in our screens (Fig. 1A, [7]),
103 this experiment was done in a Cas9 cell clone with improved gene editing compared to the
104 parental pool. Results showed that in addition to BCBL-1, BC-1, BC-2, and BC-5 require cFLIP
105 for viability. Thus, BC-1 was false negative for cFLIP dependency in our CRISPR screens. In
106 contrast, cFLIP single gene KO did not significantly affect the viability of BC-3 cells. Cell death
107 following cFLIP KO in BCBL-1/Cas9 cells was rescued by lentiviral re-expression of either major
108 cFLIP isoform (cFLIP-L and S; Figs. 1C, S1E). These data collectively confirm that cFLIP is
109 essential in the majority of PEL cell lines. The essentiality of cFLIP in BC-1 furthermore
110 suggests that expression of vFLIP may not be sufficient to overcome the requirement for cFLIP.

111 **cFLIP and vFLIP have distinct roles in PEL cell lines**

112 To further investigate whether vFLIP and cFLIP are redundant, we tested if KSHV vFLIP can
113 rescue cells from cell death after cFLIP KO. We additionally tested the viral FLIP proteins
114 encoded by molluscum contagiosum virus (MCV), MC159L or MC160L, given that KSHV vFLIP
115 and MCV MC159L and MC160L each have distinct functional activities (Fig. 2A). While either
116 major isoform of cFLIP can inhibit CASP8 and activate NF-κB signaling in ectopic contexts [12, 28,
117 29, 30], reports of KSHV vFLIP's ability to strongly inhibit CASP8 are mixed or ambiguous.
118 Conversely, MCV MC159L and MC160L both repress NF-κB signaling and only MC159L
119 inhibits CASP8 [8, 31, 32, 33]. Thus, this approach allows us to assess the redundancy of vFLIP with
120 cFLIP and the importance of NF-κB activation and CASP8 inhibition for cFLIP dependency.

121 Interestingly, we observed only partial rescue of cFLIP dependency after overexpression
122 of KSHV vFLIP (Figs. 2B, C, S2A). In contrast, overexpression of MC159L conferred complete
123 rescue, while overexpression of MC160L had no effect. Expression of each of the viral FLIP
124 proteins was comparable to overexpressed cFLIP and did not affect the expression of
125 endogenous cFLIP (Figs. S2A, B). KSHV vFLIP was furthermore overexpressed well above
126 levels of the endogenous viral protein in BC-3 (Fig. S2C). Thus, the inability of vFLIP to
127 efficiently rescue cFLIP expression is not due to lower expression relative to cFLIP or
128 endogenous vFLIP. Collectively, these results suggest that FLIP proteins that are known potent
129 inhibitors of CASP8 (cFLIP and MC159L), but not KSHV vFLIP, can efficiently rescue cFLIP
130 dependency in PEL cells. Therefore, the essential role of cFLIP in PEL cells is substantially
131 distinct from that of vFLIP.

132 **Genome-wide rescue screens uncover an ER/Golgi/CASP8-dependent death signaling**
133 **program repressed by cFLIP**

134 cFLIP has a well-characterized role in protecting cells from the effects of cell death ligands of
135 the extrinsic apoptosis pathway [9, 11]. Indeed, Epstein-Barr virus (EBV)-immortalized
136 lymphoblastoid cell lines (LCLs) depend on cFLIP expression for protection from autocrine TNF-
137 α signaling [34]. TNF-α is not expressed in PEL cell lines (Fig. S3), however. We therefore sought
138 to identify mechanisms underlying cFLIP dependency of PEL cell lines in genome-wide
139 CRISPR/Cas9 rescue screens, outlined in Fig. 3A. In these screens, sgRNAs targeting genes
140 whose inactivation overcomes cFLIP dependency should be enriched after toxic cFLIP
141 inactivation and may represent putative components of the cell death process that is inhibited by
142 cFLIP in PEL cells. We initially chose the background of BCBL-1/Cas9, which has strong cFLIP
143 dependency and excellent CRISPR/Cas9 editing efficiency. Briefly, we transduced BCBL-
144 1/Cas9 with the genome-wide Brunello sgRNA library [35] and passaged the cell population to
145 allow dropout of sgRNAs targeting essential genes. We next challenged the resulting cell pool

146 with another sgRNA vector targeting either cFLIP or the AAVS1 safe harbor locus and further
147 passaged the culture until a cFLIP-sgRNA resistant population was obtained (Fig. S4A). In an
148 independent experiment, we used three separate shRNAs for toxic cFLIP knock-down alongside
149 two negative control shRNAs targeting Renilla luciferase (RLuc) (Fig. S4B). We finally repeated
150 the sg-cFLIP resistance screen in BC-2, which has robust cFLIP dependency (Fig. 1A, B). In
151 each case, resulting cell pools were subjected to next generation sequencing of the Brunello
152 sgRNA inserts and sgRNA composition was analyzed using MAGeCK's robost ranked
153 aggregation (RRA) (Table S1). Independent shRNAs targeting either cFLIP or RLuc were
154 treated as replicates in this analysis. Results from the BCBL-1/Cas9 screens were more robust
155 than those from the BC-2 screen, which was noisy, most likely due to relatively poor editing in
156 the BC-2 Cas9 cell pool (Fig. S4C). Within BCBL-1, top hits from the shRNA-based challenge
157 were statistically more significant but had less dramatic sgRNA fold-changes (Fig. S4C). This is
158 likely due to the inclusion of three different shRNAs targeting cFLIP, each resulting in less
159 complete toxicity than the single highly efficient cFLIP sgRNA (Fig. S4A, B). To account for
160 these differences, we initially compared the BCBL-1 sgRNA and shRNA screens using a rank-
161 based filtering approach. Intersecting the top 150 hits by RRA score from the sgRNA and
162 shRNA challenge in BCBL-1 yielded 23 high-confidence hits (Fig. 3B, Table S2).

163 DAVID pathway analysis [36] shows that these high confidence hits function in three main
164 pathways (Table S3, Fig. 3C): the extrinsic apoptosis pathway (including CASP8, FADD, and
165 TNFRSF10A, encoding TRAIL receptor 1, Fig. 3D), protein modification by the ubiquitin-like
166 modifier UFM1 (UFMylation, Fig. 3E), and chondroitin sulfate proteoglycan synthesis (Fig. 3F).
167 Hits were furthermore enriched for genes associated with the ER and Golgi cellular
168 compartments (Fig. 3C). Specifically, TRAIL-R1 and CXCR4 are transmembrane receptors
169 which traffic through the ER-Golgi network. The UFMylation pathway mediates ubiquitin-fold
170 modified 1 (UFM1) conjugation to lysine residues of target proteins at the cytoplasmic surface of

171 the ER membrane [37, 38, 39, 40, 41, 42, 43]. SRP68 and SRP72 are components of the signal
172 recognition peptide (SRP) complex, which cooperates with the SEC61A translocon to aid
173 insertion of nascent transmembrane proteins into the ER [44, 45, 46] (Fig. 3E). The SRP is involved
174 in translational halting during membrane insertion [46, 47]. ER translocation of translationally
175 paused nascent peptides requires UFMylation of the 60S ribosomal protein L26 (RPL26), which
176 has been proposed as the primary target of UFM1 modification [48, 49]. Nine of the 23 high
177 confidence hits participate in the chondroitin sulfate proteoglycan synthesis pathway (Fig. 3F), a
178 process that occurs in the Golgi apparatus and involves the addition of chondroitin sulfate
179 moieties to transmembrane proteins [50]. Jagunal homolog 1 (JAGN1) is required for vesicular
180 transport from the ER or Golgi, although the exact step JAGN1 participates in is unclear [51].
181 Lastly, EHMT2 is a histone methyltransferase which has been implicated in the epigenetic
182 regulation of the UPR and/or ER homeostasis [52, 53]. A subset of these genes also scored in the
183 top 150 hits of the BC-2 screen, including CASP8 and TNFRSF10A (extrinsic apoptosis), UBA5
184 and UFSP2 (UFMylation), and UXS1, B4GALT7, CHST15, CSGALNACT1 (chondroitin sulfate
185 proteoglycan synthesis), thereby confirming these genetic interactions of cFLIP in a second PEL
186 cell line (Tables S1 and S2).

187 Consistent with our screening results, BCBL-1 CASP8 KO pools derived using two
188 different sgRNAs were completely protected from cell death after subsequent cFLIP sgRNA
189 challenge (Figs. 4; Fig. S4D). These results confirm that our screens capture CASP8 as a key
190 component of the cell death pathway that necessitates cFLIP expression in PEL cells.

191 **cFLIP protects PEL cells from ligand-independent TRAIL-R1-induced cell death**

192 In addition to *CASP8*, *TNFRSF10A,* encoding TRAIL receptor 1 (TRAIL-R1/DR4) scored highly
193 in our screens. Interestingly, neither the ligand for TRAIL-R1 (i.e. *TNFSF10* encoding TRAIL)
194 nor *TNFRSF10B*, encoding TRAIL receptor 2 (TRAIL-R2/DR5) or other death receptors were
195 hits in our screens (Table S1). As for CASP8, we generated TRAIL-R1 KO pools using two

196 independent sgRNAs (Fig. 5A). Cumulative growth curve analyses following subsequent cFLIP
197 KO confirmed that TRAIL-R1-deficient cells no longer require cFLIP expression for viability (Fig.
198 5B, Fig. S5A). TRAIL (ligand) mRNA is not well expressed in RNA-seq data from three different
199 PEL cell lines, including BCBL-1 (Fig S3). Indeed, TRAIL ELISA on cellular supernatants or
200 lysates of BCBL-1 and BC-3 cells failed to detect secreted or intracellular TRAIL [54, 55] in either
201 cell line (Fig. 5C). This assay detected levels of recombinant TRAIL well below the IC50 of
202 "TRAIL-sensitive" cell lines within the literature [56]. BCBL-1 cells are furthermore TRAIL-resistant,
203 even to hyper-physiological concentrations as high as 10 μg/mL (Fig. S5B). As additional
204 controls, we generated TRAIL and TRAIL-R2 KO pools. While NGS-based sequencing of the
205 targeted loci to characterize indel rates within our KO pools showed that >95% of each locus
206 contains inactivating indels after editing (Table S4), genetic disruption of neither locus affected
207 BCBL-1 dependency on cFLIP (Figs. 5B, S5A).

208 Ligand-independent activation of TRAIL-R2, and in some cases TRAIL-R1, has previously been
209 described within the context of ER stress-induced cell death[22, 57, 58, 59, 60]. Ligand independent
210 activation of TRAIL-R1 may furthermore be important in the context of secretory/Golgi stressors
211 [61]. Ligand independent signaling of TRAIL receptors follows their intracellular accumulation
212 rather than surface expression [61, 62]. Similarly, TRAIL-R1 in BCBL-1 is exclusively expressed
213 intracellularly in PEL cells (Figs. 5D, S5C). Based on these findings, we conclude that cFLIP
214 protects PEL cells from an intracellular, ligand-independent, TRAIL-R1-mediated cell death
215 program.

216 **UFMylation and JAGN1 promote TRAIL-R1 expression in PEL cells**

217 To extend validation of the resistance screens beyond TRAIL-R1 and CASP8, we chose two
218 hits from the UFMylation pathway (UFM1, DDRGK1), two genes from the chondroitin sulfate
219 proteoglycan synthesis pathway (UGDH, CHST15), JAGN1, and CXCR4 for single gene KO by
220 two independent sgRNAs each. Generation of an SRP68 KO cell line failed due to the

221 essentiality of this gene in PEL cells, which was unsurprising, since all six subunits of the full
222 SRP complex are pan-essential based on data from the Cancer Dependency Map (Table S2).
223 Regardless, we speculate that the screens correctly captured a biologically relevant connection
224 to the SRP, due to the functional link between the SRP and UFMylation of RPL26. The
225 essentiality of the SRP complex likely also explains why only 2 of 6 SPR complex members
226 scored in our screen (Fig. 3B). We did not attempt generating an EHMT2 KO cell pool, since
227 EHMT2 is also pan-essential and likely essential in PEL cells[7]. Western Blot analysis confirmed
228 disruption of UFMylation in UFM1 KO pools (Fig. S6A). Interestingly, DDRGK1 KO did not
229 reduce the most prominent UFM1-modified bands, suggesting that these represent upstream
230 UFMylation pathway intermediates and/or other DDRGK1-independent UFMylation events. We
231 furthermore confirmed robust editing in all cell pools by indel sequencing (Table S4). We
232 obtained significant rescue from lethal cFLIP KO challenge for every hit, as predicted by our
233 screens (Fig. 6A, Fig. S6B). UFMylation (UFM1 and DDRGK1) and JAGN1 were furthermore
234 required for expression of TRAIL-R1, a type I transmembrane protein that contains an ER signal
235 peptide (Fig. 6B). In contrast, KO of CXCR4 and chondroitin sulfate proteoglycan synthesis
236 pathway genes (UGDH, CHST15) did not affect total TRAIL-R1 or CASP8 expression (Fig. 6B).
237 Furthermore, none of the KOs we tested led to a redistribution of TRAIL-R1 to the cell surface
238 from its typical intracellular location in PEL cells, in contrast to the recently reported
239 redistribution of TNFRSF17 after SEC61A inhibition by others (Fig. S6C) [63]. In sum, our data
240 suggest that UFMylation and JAGN1 are required for TRAIL-R1 expression, while CXCR4 and
241 the chondroitin sulfate proteoglycan synthesis pathway may promote TRAIL-R1 signaling or
242 affect cFLIP essentiality by other mechanisms.

243 **Discussion**

244 Here we have distinguished the roles of KSHV vFLIP and human cFLIP in KSHV-transformed
245 PEL cell lines. While cFLIP is required for its canonical function to inhibit CASP8 downstream of

246 a death receptor signal, vFLIP was surprisingly not detected in all PEL cell lines and could not
247 fully compensate for loss of cFLIP expression. Moreover, detectable vFLIP expression
248 correlated with requirements for NF-κB-related genes, consistent with the well characterized
249 role of KSHV vFLIP as an activator of NF-κB signaling. Thus, our data demonstrate that vFLIP
250 and cFLIP have only limited functional overlap in a physiological context. Our results suggest
251 that vFLIP has either low affinity to CASP8 or cannot effectively inhibit CASP8 once bound.
252 Since we achieved very high levels of vFLIP overexpression in our rescue experiments, vFLIP
253 sequestration from CASP8 by NEMO is less likely, although possible.

254 We identified TRAIL-R1 as the critical death receptor that triggers CASP8-induced cell death in
255 the absence of cFLIP. Unlike in EBV-transformed LCLs [34], however, this process appears
256 entirely ligand-independent. Interestingly, such a ligand-independent process has been
257 described in response to ER stress-induced cell death, mainly for TRAIL-R2. A ligand
258 independent role for TRAIL-R1 has also been reported, but primarily in the context of Golgi
259 and/or secretory stressors, rather than general ER stress [22, 57, 58, 59, 60, 61]. Ligand independent
260 cell death signaling by TRAIL receptors involves their intracellular accumulation and, similarly,
261 TRAIL-R1 is detected exclusively intracellularly in PEL cells. As reported in cells treated with
262 Golgi stressors [61], we observe no involvement of TRAIL-R2. Importantly, however, our results
263 were obtained without the addition of ER/Golgi stress inducing agents and instead represent a
264 constitutively active TRAIL-R1 death signaling process in robustly growing cells. Importantly,
265 PEL cells are of post-germinal center B cell origin and terminal B cell differentiation is typically
266 accompanied by a broad expansion and alteration of the ER and Golgi. However, PEL cell lines
267 typically lack B cell surface marker and immunoglobulin expression and the status of the
268 ER/Golgi in PEL cell lines has not been investigated in depth. Interestingly, KSHV has been
269 reported to activate the UPR and dampen its downstream transcriptional response during lytic

270 reactivation and ER stress has been shown to trigger KSHV reactivation in latently infected cells
271 [64, 65].

272 In addition to TRAIL-R1, our work has implicated several other ER/Golgi resident processes in
273 cFLIP dependency. High confidence hits in our cFLIP resistance screens included most genes
274 of the UFMylation pathway. Inactivation of UFM1 or DDRGK1 reduced TRAIL-R1 expression,
275 which is likely to explain their detection in our screens. Compared to ubiquitin, UFM1 modifies
276 only few proteins. The 60S ribosomal subunit RPL26 has been proposed as the primary UFM1
277 target, where UFM1 modification promotes the processing of translationally stalled polypeptides
278 at the ER [48, 49]. While we did not directly test the role of UFM1 or RPL26 in the translation of
279 TRAIL-R1, UFMylation of RPL26 may explain the requirement for UFM1/DDRGK1 for TRAIL-R1
280 expression. UFMylation is induced in response to cellular stressors, directing nascent peptides
281 to the ER for degradation [40, 48, 49, 66, 67] and, accordingly, disruption of UFMylation has been
282 reported to induce ER stress and increase cell death [66, 68, 69]. Of note, genes in the UFMylation
283 pathway do not score as essential in our original PEL screens and their essentiality within the
284 Cancer Dependency Map is mixed [7, 70]. Thus, it is plausible that UFMylation could similarly allow
285 translation of pro-apoptotic proteins, like TRAIL-R1, to proceed. A varied requirement for
286 UFMylation for cellular survival is further supported by findings that deletion of DDRGK1 in
287 mouse plasma cells did not result in increased cell death [71].

288 Like UFMylation, we observed that JAGN1 promotes expression of TRAIL-R1. While little is
289 known about this gene, JAGN1 has been shown to participate in the secretory pathway in
290 myeloid cells and antibody-producing B cells [51, 72]. As with UFMylation, JAGN1 is increased in
291 response to ER stress and its depletion has been linked to increased apoptosis in granulocytes
292 [51, 73]. Importantly, our PEL CRISPR screens and establishment of a JAGN1 KO cell line suggest
293 that JAGN1 is non-essential in PEL cells. Similarly, the Cancer Dependency Map indicates that
294 JAGN1 is not broadly required for cellular survival [7, 70].

295 Finally, our data suggest that chondroitin sulfate proteoglycan biosynthesis and CXCR4 are
296 involved in the ligand-independent activity of TRAIL-R1. Since inactivation of neither pathway
297 affected TRAIL-R1 expression or cause re-distribution of TRAIL-R1 to the cell surface, the exact
298 mechanism underlying their link to TRAIL-R1 signaling and cFLIP dependency remains unclear.
299 Interestingly, both CXCR4 and its primary ligand, CXCL12, have been identified as targets of
300 chondroitin sulfate moieties, although the roles of these modifications remain unclear [74, 75].
301 Additionally, there is a report of CXCR4-induced apoptosis, but this process was independent of
302 CASP8 and could not be inhibited by MC159L, unlike the TRAIL-R1 dependent process that is
303 inhibited by cFLIP in PEL cells [76].

304 In sum, our data strongly support a role for TRAIL-R1 in incorporating multiple ER/Golgi-
305 associated signals in PEL cells into a constitutive, ligand-independent cell death process that
306 must be inhibited by cFLIP to allow for cellular viability.

307

308 **Materials and Methods**

309 **Cloning**

310 Sequences for oligonucleotides and synthetic DNA fragments can be found in Supplementary
311 Table 5A and 5B. All new vectors were confirmed by Sanger sequencing (ACGT, Inc.).
312 pLenti SpBsmBI sgRNA Hygro (Addgene, 62205) constructs were cloned by ligating annealed
313 oligonucleotides specified in Supplemental Table 5C with the BsmBI-digested vector [77].
314 For rescue experiments, human C-terminally 3X-FLAG tagged FLIP long and short isoforms and
315 KSHV vFLIP were ordered as codon-optimized dsDNA gene fragment blocks (Integrated DNA
316 Technologies). This initial codon optimization introduced resistance to cFLIP sg1, while cFLIP
317 sg2 resistance was introduced via two overlapping PCRs centered on the sg2 target site using
318 the synthetic gene fragment as a template (primers 4672/4673 and 4674/4323). PCR products

319 were then inserted between the AgeI and BamHI sites of vector pLC-IRES-HYG [78] using Gibson
320 assembly. KSHV vFLIP was cloned from a codon-optimized gene fragment block containing the
321 entire vCyclin/vFLIP locus using primers 4317/4318 and Gibson assembled with 3X-FLAG PCR
322 products amplified from the cFLIP-S gene fragment (primers 4319/4323). PCR products
323 containing MC159L (primers 4338/4339) and MC160L (primers 4340/4341) were amplified from
324 pBabe-based vectors kindly provided by Dr. Joanna Shisler (UIUC) and Gibson assembled with
325 3X-FLAG PCR products amplified from the cFLIP-S gene fragment (primers 4342/4323 for
326 MC159L or 4343/4323 for MC160L).
327 vCyc and vFLIP expression constructs for transfection into 293T in Fig. S1A were cloned into
328 pMSCVpuro (Takara, Catalog # 631461) by PCR, using primers 3646/3647 (vCyc) and
329 3648/3649 (vFLIP), followed by Gibson assembly with the EcoRI/XhoI digested vector.

330 LentiGuide-Puro expressing cFLIP sg2 was cloned by ligation of annealed oligos 4532/4533
331 with BsmBI-linearized vector as described [7].

332 The parental shR-miR expression vector pZIP-ZsGreen-T2A-Hyg-shNT4 was cloned by
333 replacing the EcoRI-IRES-PuroR-NotI cassette of shERWOOD-UltramiR Lentiviral shRNA NT
334 control #4 in pZIP-hCMV-ZsGreen-Puro (Transomic) with a PCR product containing a T2A-
335 HygR cassette that was amplified using primers 3551/3552 and template lenti MS2-P65-
336 HSF1_Hygro (Addgene Plasmid #61426). The initial control insert shRNA NT control #4 was
337 replaced by digesting pZIP-ZsGreen-T2A-Hyg-shNT4 with NotI and MluI and inserting miR-30-
338 based shRNAs for cFLIP (sh1, shM, shN) or negative control shRNAs targeting Renilla
339 Luciferase (REN.308 and Ren.713) using Gibson Assembly. These shRNAs were designed
340 using SplashRNA and/or previously published [79]. dsDNA fragments specified in Table S5 were
341 ordered and used for Gibson Assembly, either directly (shM, N) or after PCR-amplification with
342 primers 4594/4607 (sh1, Ren.308, Ren.713).

343 **Western blotting**

344 Cells were pelleted, washed in ice-cold PBS, in some cases stored at -80°C, and lysed for 30
345 minutes in ice-cold RIPA buffer containing 1X protease inhibitor cocktail (Sigma-Aldrich, catalog
346 P8340). Lysates were then subjected to five cycles (30 seconds on/30 seconds off) of
347 sonication at 4 °C on high intensity in a Bioruptor Sonication System (Diagenode) and
348 subsequently cleared by centrifugation at 14,000g for 15 minutes. Lysates were diluted 5 to 10-
349 fold and quantified by Pierce BCA Protein Assay (ThermoFisher Scientific, 23225). Lysates
350 were denatured by heating at 70°C for 10 minutes 1X LDS buffer (ThermoFisher, NP0008)
351 containing a final concentration of 2.5% beta mercaptoethanol and loaded onto Bolt 4-12% Bis-
352 Tris gels (ThermoFisher Scientific; NW0412) at equivalent concentrations (15-20 µg for cFLIP
353 knockout validation based on available lysates; 50 µg for vCyc/vFLIP, and 20-30 µg for all other
354 proteins). SDS-PAGE was performed in 1X MES buffer and proteins were transferred onto
355 0.2 µm nitrocellulose membranes (Bio-Rad, 1620112).
356 Membranes were blocked at room temperature for 1 hour and probed overnight at 4 °C with
357 primary antibodies at the concentrations indicated in Table S5D. Images were captured on an
358 Odyssey FC (LI-COR Biosciences) after incubation with IRDye 800CW secondary antibodies
359 (LI-COR Biosciences) at a 1:15000 concentration. In some cases, anti-rat HRP (Santa Cruz) at
360 a 1:5000 concentration was used for detection and developed using SuperSignal West Femto
361 Maximum Sensitivity Substrate (ThermoFisher Scientific, 34094) following manufacturer
362 protocol. Contrast/brightness was dynamically adjusted as needed using ImageStudio. Bands
363 were quantified in ImageStudio Lite version 5.2 (LI-COR Biosciences). Original Western Data
364 are included as one supplemental file.

365 **Cell culture**

366 PEL and/or BJAB cell lines were maintained in RPMI 1640 with L-glutamine (Corning,
367 MT10040CM) supplemented with 10% (BC-1, BCBL-1) or 20% (BC-2, BC-3, BC-5, BJAB)
368 Serum Plus-II (Sigma-Aldrich, catalog number 14009C, lots 15H243 and 21C421), 10 µg/mL

369 gentamycin (ThermoFisher, 15710064) and 0.05 mM β-mercaptoethanol (Sigma-Aldrich,
370 M3148-25ML). HEK293T cells were maintained in DMEM (Sigma-Aldrich, D5796)
371 supplemented with 10% Serum Plus-II and 10 mg/mL gentamycin. PEL cells were counted by
372 trypan exclusion and split every second day to approximately $2x10^5$ cells/mL (or $3x10^5$ for BC-
373 5). 293T cells were maintained at visually sub-confluent densities and split every 2 days. PEL
374 cell lines expressing lentiCas9-Blast (Addgene, 52962) were previously generated and validated
375 by STR profiling [7]. The BC-1/Cas9 clonal cell line utilized in Fig. 1B was subcloned and selected
376 for editing efficiency compared to the parental Cas9 BC-1 pool utilized in the screens. This BC-
377 1/Cas9 clone was re-confirmed by STR profiling.

378 For cellular growth curves and functional titration of lentivirus other than pZIP-based vectors
379 (see below), cells were counted by flow cytometry using spike-in of a known amount of
380 AccuCount Blank Particles 5-5.9 µm (Spherotech, ACBP-50-10) as previously described [7].

381 **Cumulative cellular growth curves**

382 Importantly, all lentiviral vectors used for growth curves analyses were titrated in naïve parental
383 cell lines to ensure comparable titers between control sgRNAs and toxic sgRNAs. For growth
384 curves, cells were plated at a density of $3x10^5$ cells/mL and transduced at the MOIs indicated in
385 the text or figure legends. Medium was exchanged one day after transduction and cells were
386 selected with 1.2 µg /ml puromycin for 2 days; 200 µg /ml hygromycin for 3 days (titrations) or 5-
387 7 days (stable cell line production). Every second day, cells were counted by flow cytometry as
388 described above and then split to a density of $2x10^5$ cells/ml. This process was repeated until
389 cells that had received toxic sgRNAs were too sparse to split or for up to 10 days. Cumulative
390 cell counts were calculated by taking the measured cell concentration at a given timepoint
391 multiplied by the product of all previous dilution factors and normalized to cumulative cell counts
392 obtained for the sgAAVS1 control.

393 Statistical testing for reduced cellular viability was performed using one-sided, one-sample t-
394 testing (H_0: P(μ=1) with H_A: P(μ<1)). For rescue growth curve experiments (i.e. in the context of
395 ectopic FLIP expression or a knockout cell pool) an additional one-sided, independent two-
396 sample t-test was performed, comparing the relative cumulative cell counts for each guide
397 between the experimental cell line and the control line (i.e. sgAAVS1-Hygro or ZsGreen-Hygro).
398 In the case of ZsGreen or KSHV vFLIP expression for rescue experiments, where n= 3-6 was
399 obtained for up to day 10 (Fig. 2C), ordinary least squares regression lines were fit. Cumulative
400 cell counts relative to cell-line matched sgAAVS1 were used as the singular dependent variable
401 with one or two predictor variables. To measure depletion, data was subset on the indicated cell
402 line (ZsGreen or vFLIP expression) and sgRNA (sgPSM1 or cFLIP sg1) with the timepoint (>0
403 days after transduction) as a singular predictor variable. To measure rescue, data was subset
404 on a particular sgRNA (sgPSMD1 or cFLIP sg1) with the cell line (ZsGreen or vFLIP) as an
405 additional categorical predictor variable besides the timepoint (2-8 days post-transduction). A
406 one-sided t-test was then used to determine whether the coefficients for day (depletion) or cell
407 line (rescue) were < or > 0, respectively.

408 **Lentiviral production, infection, and titration**

409 Except for pZIP-based vectors, lentivirus was produced using packaging plasmids psPAX2,
410 pMD2.G, and transfer vectors at 1.3:0.72:1.64 molar ratios. HEK293T Cells were seeded at a
411 density of 1.25×10^7 per 15-cm dish and transfected with 30 μg of DNA using a 1:3 to 1:3.5 ratio
412 of μg of DNA to μL PEI. Media were replaced after ~6 hours and cell supernatants containing
413 viral vectors were collected 48-72 hours later and filtered through 450nm pore size filters. Viral
414 vector preparations were used as is or concentrated by ultracentrifugation or using Amicon Ultra
415 Centrifugal Filter Units (Millipore, UFC910024) following manufacturer protocol. In some cases,
416 lentivirus was stored at -80°C.

417 Lentiviral vector titers were measured using functional titration of serially diluted viral stocks.
418 The multiplicity of infection (MOI) of each dilution point was estimated using the percentage of
419 live cells relative to an untreated control and a resulting viral concentration (transducing
420 units/mL) was calculated from the average of multiple dilution points assuming a Poisson
421 distribution, $P(x) = \frac{\lambda^x e^{-\lambda x}}{x!}$, to estimate the mean event rate λ (MOI) assuming P(x=0) is the
422 percentage of uninfected cells.

423 Transductions were carried out at $3x10^5$ cells/ml and the indicated MOIs under normal culture
424 conditions supplemented with 5 µg/mL polybrene (Sigma-Aldrich, TR-1003-G). Culture medium
425 was replaced ~24 hours after transduction and antibiotic resistance selection was carried out
426 using 1.2 µg/ml puromycin for 2 days; 200 µg /ml hygromycin for 3 days (titrations) or 5-7 days
427 (stable cell line production and CRISPR screens).

428 Procedures for pZIP-ZsGreen-T2A-Hygro shRNA vectors are described below.

429 **CRISPR-based single-gene knockout**

430 CRISPR knockout was achieved by transduction of published Cas9-expressing cell pools or
431 clones and published lentiviral single guide RNA constructs for AAVS1, PSMD1 sg1, IRF4 sg1,
432 cFLIP sg1. A new cFLIP sg2 was cloned for this paper since sg2 from the previous study
433 performed sub-optimally. The new cFLIP sg2 corresponds to sgRNA 2 (by rule set 2 score, on
434 target activity) from the Brunello library. sgRNAs in pLentiGuide-Puro (Addgene, 52963) were
435 used for cumulative growth curve knockout, while long-term single-gene knockout cell lines
436 were generated using sgRNAs in pLenti SpBsmBI sgRNA Hygro (Addgene, 62205) containing a
437 hygromycin resistance cassette. Sequences of all sgRNAs can be found in Table S5C.

438 **CRISPR-based synthetic rescue screens with sgRNA challenge**

439 Library virus was generated and titrated as described above using the Brunello sgRNA pool
440 library in lentiGuide-Puro (Addgene, 73178). In all cases, approximately $9.2x10^7$ to $1.5x10^8$ cells
441 were transduced at an MOI of 0.3 to result in a single sgRNA per cell at a coverage of 300-500X
442 cells per guide. Transduced cells were selected using 1.2 μg/ml puromycin, and dropout was
443 allowed to proceed for 12 days with at least $3.6x10^7$ cells maintained to preserve library
444 complexity.

445 The resulting cell pool was then challenged with either cFLIP sg1 or the negative control
446 sgAAVS1 in pLenti SpBsmBI sgRNA Hygro at an MOI < 0.5. Cells were selected with
447 hygromycin and cultured until resistance to cFLIP knockout was apparent by cellular
448 proliferation, i.e. until day 12 after sgRNA transduction. At this point, approximately $3\text{-}7x10^8$ cells
449 (500-1000X coverage) were harvested, washed in ice-cold PBS, and snap frozen.

450 **shRNA-based synthetic rescue screens**

451 pZIP transfer vectors were packaged in Lenti-X 293T cells (Takara) using molar ratios of 0.2
452 transfer vector to 0.51 psPax2 to 0.29 pMD2.G. Briefly, $2.1x10^7$ pLenti-X 293T cells/15 cm dish
453 were transfected with ~48.5 μg total plasmid and supernatant was harvested 48 hours later
454 without replacing media. Supernatants were filtered through 450nm pore size filters and
455 concentrated by ultracentrifugation (Beckman SW32Ti, 25,000 rpm, 90 min), resuspend in
456 OptiMEM on a platform shaker for at least 60 min at 4°C and followed by pipetting up and down
457 20 times, aliquoted, and snap frozen at -80°C. Virus aliquots were thawed at 37°C and cleared
458 by centrifugation at 400 g for 5 min before use. Titration of the negative control vectors was
459 performed based on ZsGreen expression and flow cytometry in BCBL1/Cas9 clone C2. Titration
460 of the toxic cFLIP shRNAs was performed in 293T cells lacking Dicer (293T/NoDice) [80], relative
461 to a negative control with known titer in BCBL1/Cas9.

462 BCBL1/Cas9 Brunello library transduction was performed at MOI 0.3 in eleven 15 cm dishes at
463 $5x10^5$ cells/ml and 50ml/dish, ~920x theoretical sgRNA coverage. Cells were selected using 1.2
464 μg/ml puromycin from days 1 to 4 after transduction and expanded. On Day 9 after Brunello
465 transduction, seven 15 cm dishes of cells ($3x10^5$ cells/ml and 50 ml/dish) were challenged with
466 each shRNA vector at MOI 0.5. The next day, cells were collected by centrifugation and
467 resuspended in fresh medium containing 200μg/ml Hygromycin. Cell pools were maintained at
468 coverage and optimal cell density with hygromycin for one week and at least $4x10^7$
469 cells/condition were harvested on day 12 into the shRNA challenge.

470 **CRISPR library preparation and next-generation sequencing**

471 Genomic DNA was isolated following a previously described protocol and library preparation
472 was performed as previously described for sgRNA and shRNA screens in BCBL-1 [7]. Resulting
473 libraries were quantified by Qubit (ThermoFisher Scientific, Q33231) prior to further QC and
474 quantification by Bioanalyzer (Agilent) and Kapa qPCR (Roche). Multiplexing of sgRNA
475 challenge screens in BCBL-1 was performed utilizing 6-bp indexes and sequenced on a single
476 lane of a HiSeq4000 (Illumina) using 50bp single-end (SE) reads with 10% PhiX spike-in as
477 previously described [7]. For sgRNA challenge screens in BC-2, sequencing was performed on a
478 single flow-cell of an NextSeq 500 (Illumina) using 75bp SE reads with 10% PhiX spike-in due to
479 the discontinuation of the HiSeq4000 platform. For these runs, library preparation was modified
480 slightly to combine genomic amplification and addition of adapters/barcode into a single PCR
481 step with custom 8bp indexes (sequences can be found in Supplementary Table 5E). The
482 shRNA-based screens were prepped and sequenced twice as a quality control using both
483 approaches/platforms and reads were subsequently merged for further analysis. Demultiplexed
484 reads have been deposited on GEO (accession GSE210445).

485 5' adapters were trimmed from raw CRISPR sequencing reads and trimmed to length (20 bp)
486 from the 3' end using Cutadapt v4.1 [81]. Reads were then aligned using Bowtie v1.1.2 9 [82].

487 Guide-level counts were obtained using MAGeCK v0.5.9 and statistical testing was performed
488 using MAGeCK's robust rank aggregation (RRA) algorithm using median normalization [83].

489 **CRISPR Knockout Pools Indel Sequencing**

490 A 200-300 bp region around each indicated guide was amplified from genomic DNA using the
491 primers indicated in Supplemental Table 5F and sent to Massachusetts General Hospital CCIB
492 DNA Core for low depth sequencing. Raw FASTQ files were assembled into contigs by MGH
493 and the resulting effect on the coding sequence was determined using custom alignment and
494 classification script built using Biopython [84] to estimate indel, frameshift, and early stopping
495 incidence. Briefly, assembled contigs were aligned to the coding sequences targeted by each
496 amplicon to determine optimal positioning of the contig in reference to the full coding sequence.
497 All alignments utilized a simple pairwise scoring matrix (+1 for matches, +0 for mismatches, -.99
498 for gap opening, and -0 for gap extensions) chosen by iterative manual assessment of the
499 collective results for the most abundant contig for each gene. The resulting, fully assembled
500 coding sequence was then classified as an indel or non-indel for all sequences. Indels were
501 further characterized as in-fame or frameshifted based on the number of nucleotides lost or
502 gained across all alignment gaps. Early stopping events for all variants were predicted by *in*
503 *silico* translation of predicting coding sequences. Raw FASTQ output was also analyzed using
504 CRISPResso2 [85] to obtain estimates of the number of modified and frameshifted reads.

505 **mRNA Sequencing**

506 A frozen BC1 lysate in Trizol was submitted to BGI Group (Shenzhen, China) for single-ended,
507 polyA-enriched RNA sequencing. Un-trimmed reads were aligned to the Gencode 41 annotation
508 of GRCh38.p13 with STAR v2.7.10. Raw sequencing data has been made available on GEO
509 (accession GSE210446).

510 **Cellular staining and flow cytometry**

511 Cells were washed twice in ice-cold PBS and APC Annexin V (BD Biosciences, 550475) and 7-
512 AAD (BD Biosciences, 559925) staining was performed on $1x10^5$ in 100 μL of 1X Annexin V
513 binding buffer (BD Biosciences, 556454) following manufacturer recommended guidelines,
514 using 5 μL of each stain for 15 minutes at room temperature in the dark. Necrotic cells were
515 generated for Annexin V and 7-AAD compensation controls using a 30-minute heat shock at
516 95°C. Stained cells were diluted with 400 μL 1x Annexin V binding buffer and flow cytometry
517 was performed on a BD FACSCanto II (BD Biosciences) within 1 hour.

518 For TRAIL-R1 staining, cells were harvested and washed twice in ice-cold PBS and
519 resuspended in PBS at a concentration of $1x10^6$ cells/mL. 500 μL of cells were then fixed in
520 PBS containing 4% w/v PFA for 10 minutes followed by two more PBS washes. On the final
521 wash, cells were split into two and each resuspended in 250 μL PBS containing 1% w/v bovine
522 serum albumin (Sigma, 10735078001) with or without the addition of 0.1% w/v saponin (Sigma-
523 Aldrich, 47036). Cells were pre-incubated for 15 minutes at room temperature with 250 μL
524 PBS/1% BSA with or without 0.1% w/v saponin, containing 1:400 of Human BD Fc Block
525 (ThermoFisher Scientific, BDB564219) per condition, followed by addition of 1:100 (2.5 μL in
526 250 μL) of FITC-conjugated Anti-TRAIL receptor 1 (Abcam, ab59047; specific to the
527 extracellular domain of TRAIL-R1) for 30 minutes at room temperature in the dark. Cells were
528 then washed 3X with PBS/1% BSA with or without 0.1% w/v saponin followed by a final re-
529 suspension in 500 μL PBS containing .01% PFA.

530 Stained cells were stored for up to 2 days at 4 °C in the dark (TRAIL-R1) and flow cytometry
531 was performed on a BD FACSCanto II (BD Biosciences). Raw data were exported to FlowJo
532 v10.8.1 for analysis and plotting.

533 **Enzyme-linked immunosorbent assay**

534 Anti-TRAIL ELISA was performed using a Human TRAIL/TNFSF10 Quantikine ELISA Kit (R&D
535 Systems, DTRL00) following manufacturer-provided protocols. Briefly, 50 μL of cell supernatant
536 or cellular lysate obtained using manufacturer provided buffers and instructions were added to
537 each well. Cell densities at time of harvesting were $8x10^6$ to $1.2x10^7$ PEL cells, while cells were
538 lysed at a concentration of $1x10^7$ cells/mL as per manufacturer guidelines. The included
539 recombinant human TRAIL standard (R&D Systems, 892375) was serially diluted in 2-fold steps
540 from 1000 to 15.6 pg/mL. Absorbance was read on a VICTOR Nivo Plate reader at 450 nm. A
541 blank measurement taken from a well containing clean dilution buffer was subtracted from all
542 other wells and least squares regression was performed on the measured values across all
543 replicates to determine effective concentrations.

544 **In vitro TRAIL treatment**

545 BCBL-1/Cas9 cells containing pLenti SpBsmBI Guide Hygro (AAVS1 or TRAIL-R1 #1/2) were
546 treated with the indicated serial dilutions of recombinant human TRAIL (Sigma-Aldrich, T9701)
547 and absolute cell numbers were measured 24 hours later by flow cytometry as described above
548 for cumulative growth curves.

549 **Statistical Analysis**

550 Statistical testing/modeling was conducted in Python using SciPy 1.6.0[86] (simple t tests) or
551 Statsmodels 0.13.2 (ordinary least squares) unless otherwise indicated. Vertical bar graphs
552 were generated using Prism 9.4.1 (GraphPad), all other figures were generated using Seaborn
553 0.11.2 [87]. Full code for computational and statistical analyses was made available online on
554 Github (https://github.com/Gottwein-Lab).

555 **Acknowledgements**

556 We would like to thank Dr. Joanna Shisler for sharing MCV FLIP protein expression vectors and
557 Dr. Ethel Cesarman for sharing a control aliquot of BC-3 cells.

558 **Competing Interests** The authors do not have competing interests.

559 **Author Contributions** Study Design NK, MM, and EG. MM performed exploratory resistance
560 screens in BC-3, which were not included in the final manuscript due to very low cFLIP
561 dependency of this cell line. NK performed all experiments, except shRNA vector cloning and
562 shRNA resistance screens until harvest of cell pellets, which were performed by EG.
563 Computational and statistical analyses were performed by NK. NK put together figures, which
564 were edited by EG. NK and EG wrote the manuscript. EG supervised all aspects of the work. All
565 authors read and approved the final manuscript.

566 **Ethics Statement** This study did not require ethical approval.

567 **Funding** This work was supported by NCI R01 CA247619 and R01 CA247619-01A1S1 to E.G.;
568 MM was supported by K22 CA241355.

569 **Data Availability** CRISPR screening and RNAseq data were deposited on GEO (accessions
570 GSE210445, GSE210446). All cell lines and plasmids are available on request.

571

572 **References**

573 1. Cesarman E, Chang Y, Moore PS, Said JW, Knowles DM. Kaposi's sarcoma-associated
574 herpesvirus-like DNA sequences in AIDS-related body-cavity-based lymphomas. *N Engl*
575 *J Med* 1995, **332**(18)**:** 1186-1191.

576

577 2. Nador RG, Cesarman E, Chadburn A, Dawson DB, Ansari MQ, Sald J*, et al.* Primary
578 effusion lymphoma: a distinct clinicopathologic entity associated with the Kaposi's
579 sarcoma-associated herpes virus. *Blood* 1996, **88**(2)**:** 645-656.

580

581 3. Lurain K, Polizzotto MN, Aleman K, Bhutani M, Wyvill KM, Goncalves PH*, et al.* Viral,
582 immunologic, and clinical features of primary effusion lymphoma. *Blood* 2019, **133**(16)**:**
583 1753-1761.

584

585 4. Wies E, Mori Y, Hahn A, Kremmer E, Sturzl M, Fleckenstein B*, et al.* The viral interferon-
586 regulatory factor-3 is required for the survival of KSHV-infected primary effusion
587 lymphoma cells. *Blood* 2008, **111**(1)**:** 320-327.

588

589 5. Godfrey A, Anderson J, Papanastasiou A, Takeuchi Y, Boshoff C. Inhibiting primary
590 effusion lymphoma by lentiviral vectors encoding short hairpin RNA. *Blood* 2005, **105**(6)**:**
591 2510-2518.

592

593 6. Chaudhary PM, Jasmin A, Eby MT, Hood L. Modulation of the NF-kappa B pathway by
594 virally encoded death effector domains-containing proteins. *Oncogene* 1999, **18**(42)**:**
595 5738-5746.

596

597 7. Manzano M, Patil A, Waldrop A, Dave SS, Behdad A, Gottwein E. Gene essentiality
598 landscape and druggable oncogenic dependencies in herpesviral primary effusion
599 lymphoma. *Nat Commun* 2018, **9**(1)**:** 3263.

600

601 8. Hu S, Vincenz C, Buller M, Dixit VM. A novel family of viral death effector domain-
602 containing molecules that inhibit both CD-95- and tumor necrosis factor receptor-1-
603 induced apoptosis. *J Biol Chem* 1997, **272**(15)**:** 9621-9624.

604

605 9. Irmler M, Thome M, Hahne M, Schneider P, Hofmann K, Steiner V*, et al.* Inhibition of
606 death receptor signals by cellular FLIP. *Nature* 1997, **388**(6638)**:** 190-195.

607

608 10. Thome M, Schneider P, Hofmann K, Fickenscher H, Meinl E, Neipel F*, et al.* Viral
609 FLICE-inhibitory proteins (FLIPs) prevent apoptosis induced by death receptors. *Nature*
610 1997, **386**(6624)**:** 517-521.

611

612 11. Krueger A, Schmitz I, Baumann S, Krammer PH, Kirchhoff S. Cellular FLICE-inhibitory
613 protein splice variants inhibit different steps of caspase-8 activation at the CD95 death-
614 inducing signaling complex. *J Biol Chem* 2001, **276**(23)**:** 20633-20640.

615

616 12. Kataoka T, Budd RC, Holler N, Thome M, Martinon F, Irmler M*, et al.* The caspase-8
617 inhibitor FLIP promotes activation of NF-kappaB and Erk signaling pathways. *Curr Biol*
618 2000, **10**(11)**:** 640-648.

619

620 13. Chugh P, Matta H, Schamus S, Zachariah S, Kumar A, Richardson JA*, et al.*
621 Constitutive NF-κB activation, normal Fas-induced apoptosis, and increased incidence of
622 lymphoma in human herpes virus 8 K13 transgenic mice. *Proceedings of the National*
623 *Academy of Sciences of the United States of America* 2005, **102**(36)**:** 12885-12890.

624

625 14. Bélanger C, Gravel A, Tomoiu A, Janelle ME, Gosselin J, Tremblay MJ*, et al.* Human
626 herpesvirus 8 viral FLICE-inhibitory protein inhibits Fas-mediated apoptosis through
627 binding and prevention of procaspase-8 maturation. *J Hum Virol* 2001, **4**(2)**:** 62-73.

628

629 15. Tolani B, Matta H, Gopalakrishnan R, Punj V, Chaudhary PM. NEMO is essential for
630 Kaposi's sarcoma-associated herpesvirus-encoded vFLIP K13-induced gene expression
631 and protection against death receptor-induced cell death, and its N-terminal 251
632 residues are sufficient for this process. *J Virol* 2014, **88**(11)**:** 6345-6354.

633

634 16. Galluzzi L, Vitale I, Aaronson SA, Abrams JM, Adam D, Agostinis P*, et al.* Molecular
635 mechanisms of cell death: recommendations of the Nomenclature Committee on Cell
636 Death 2018. *Cell Death & Differentiation* 2018, **25**(3)**:** 486-541.

637

638 17. Fritsch M, Gunther SD, Schwarzer R, Albert MC, Schorn F, Werthenbach JP*, et al.*
639 Caspase-8 is the molecular switch for apoptosis, necroptosis and pyroptosis. *Nature*
640 2019, **575**(7784)**:** 683-687.

641

642 18. Newton K, Wickliffe KE, Maltzman A, Dugger DL, Reja R, Zhang Y*, et al.* Activity of
643 caspase-8 determines plasticity between cell death pathways. *Nature* 2019, **575**(7784)**:**
644 679-682.

645

646 19. Yu L, Alva A, Su H, Dutt P, Freundt E, Welsh S*, et al.* Regulation of an ATG7-beclin 1
647 program of autophagic cell death by caspase-8. *Science* 2004, **304**(5676)**:** 1500-1502.

648

649 20. Bell BD, Leverrier S, Weist BM, Newton RH, Arechiga AF, Luhrs KA*, et al.* FADD and
650 caspase-8 control the outcome of autophagic signaling in proliferating T cells. *Proc Natl*
651 *Acad Sci U S A* 2008, **105**(43)**:** 16677-16682.

652

653 21. Jimbo A, Fujita E, Kouroku Y, Ohnishi J, Inohara N, Kuida K*, et al.* ER stress induces
654 caspase-8 activation, stimulating cytochrome c release and caspase-9 activation. *Exp*
655 *Cell Res* 2003, **283**(2)**:** 156-166.

656

657 22. Munoz-Pinedo C, Lopez-Rivas A. A role for caspase-8 and TRAIL-R2/DR5 in ER-stress-
658 induced apoptosis. *Cell Death Differ* 2018, **25**(1)**:** 226.

659

660 23. Grundhoff A, Ganem D. Mechanisms governing expression of the v-FLIP gene of
661 Kaposi's sarcoma-associated herpesvirus. *J Virol* 2001, **75**(4)**:** 1857-1863.

662

663 24. Liu L, Eby MT, Rathore N, Sinha SK, Kumar A, Chaudhary PM. The human herpes virus
664 8-encoded viral FLICE inhibitory protein physically associates with and persistently
665 activates the Ikappa B kinase complex. *J Biol Chem* 2002, **277**(16)**:** 13745-13751.

666

667 25. Field N, Low W, Daniels M, Howell S, Daviet L, Boshoff C*, et al.* KSHV vFLIP binds to
668 IKK-gamma to activate IKK. *J Cell Sci* 2003, **116**(Pt 18)**:** 3721-3728.

669

670 26. Sun Q, Matta H, Chaudhary PM. The human herpes virus 8-encoded viral FLICE
671 inhibitory protein protects against growth factor withdrawal-induced apoptosis via NF-
672 kappa B activation. *Blood* 2003, **101**(5)**:** 1956-1961.

673

674 27. Bagneris C, Rogala KB, Baratchian M, Zamfir V, Kunze MB, Dagless S*, et al.* Probing
675 the Solution Structure of IkappaB Kinase (IKK) Subunit gamma and Its Interaction with

676 Kaposi Sarcoma-associated Herpes Virus Flice-interacting Protein and IKK Subunit beta
677 by EPR Spectroscopy. *J Biol Chem* 2015, **290**(27)**:** 16539-16549.

678

679 28. Hu WH, Johnson H, Shu HB. Activation of NF-kappaB by FADD, Casper, and caspase-
680 8. *J Biol Chem* 2000, **275**(15)**:** 10838-10844.

681

682 29. Kataoka T, Tschopp J. N-terminal fragment of c-FLIP(L) processed by caspase 8
683 specifically interacts with TRAF2 and induces activation of the NF-kappaB signaling
684 pathway. *Mol Cell Biol* 2004, **24**(7)**:** 2627-2636.

685

686 30. Baratchian M, Davis CA, Shimizu A, Escors D, Bagneris C, Barrett T*, et al.* Distinct
687 Activation Mechanisms of NF-kappaB Regulator Inhibitor of NF-kappaB Kinase (IKK) by
688 Isoforms of the Cell Death Regulator Cellular FLICE-like Inhibitory Protein (cFLIP). *J Biol*
689 *Chem* 2016, **291**(14)**:** 7608-7620.

690

691 31. Shisler JL, Moss B. Molluscum contagiosum virus inhibitors of apoptosis: The MC159 v-
692 FLIP protein blocks Fas-induced activation of procaspases and degradation of the
693 related MC160 protein. *Virology* 2001, **282**(1)**:** 14-25.

694

695 32. Nichols DB, Shisler JL. The MC160 protein expressed by the dermatotropic poxvirus
696 molluscum contagiosum virus prevents tumor necrosis factor alpha-induced NF-kappaB
697 activation via inhibition of I kappa kinase complex formation. *J Virol* 2006, **80**(2)**:** 578-
698 586.

699

700 33. Biswas S, Smith GL, Roy EJ, Ward B, Shisler JL. A comparison of the effect of
701 molluscum contagiosum virus MC159 and MC160 proteins on vaccinia virus virulence in
702 intranasal and intradermal infection routes. *J Gen Virol* 2018, **99**(2)**:** 246-252.

703

704 34. Ma Y, Walsh MJ, Bernhardt K, Ashbaugh CW, Trudeau SJ, Ashbaugh IY*, et al.*
705 CRISPR/Cas9 Screens Reveal Epstein-Barr Virus-Transformed B Cell Host
706 Dependency Factors. *Cell Host Microbe* 2017, **21**(5)**:** 580-591.e587.

707

708 35. Doench JG, Fusi N, Sullender M, Hegde M, Vaimberg EW, Donovan KF*, et al.*
709 Optimized sgRNA design to maximize activity and minimize off-target effects of
710 CRISPR-Cas9. *Nat Biotechnol* 2016, **34**(2)**:** 184-191.

711

712 36. Sherman BT, Hao M, Qiu J, Jiao X, Baseler MW, Lane HC*, et al.* DAVID: a web server
713 for functional enrichment analysis and functional annotation of gene lists (2021 update).
714 *Nucleic Acids Res* 2022, **50**(W1)**:** W216-221.

715

716 37. Komatsu M, Chiba T, Tatsumi K, Iemura S, Tanida I, Okazaki N*, et al.* A novel protein-
717 conjugating system for Ufm1, a ubiquitin-fold modifier. *Embo j* 2004, **23**(9)**:** 1977-1986.

718

719 38. Kang SH, Kim GR, Seong M, Baek SH, Seol JH, Bang OS*, et al.* Two novel ubiquitin-
720 fold modifier 1 (Ufm1)-specific proteases, UfSP1 and UfSP2. *J Biol Chem* 2007, **282**(8)**:**
721 5256-5262.

722

723 39. Tatsumi K, Sou YS, Tada N, Nakamura E, Iemura S, Natsume T*, et al.* A novel type of
724 E3 ligase for the Ufm1 conjugation system. *J Biol Chem* 2010, **285**(8)**:** 5417-5427.

725

726 40. Lemaire K, Moura RF, Granvik M, Igoillo-Esteve M, Hohmeier HE, Hendrickx N*, et al.*
727 Ubiquitin fold modifier 1 (UFM1) and its target UFBP1 protect pancreatic beta cells from
728 ER stress-induced apoptosis. *PLoS One* 2011, **6**(4)**:** e18517.

729

730 41. Chen C, Itakura E, Weber KP, Hegde RS, de Bono M. An ER complex of ODR-4 and
731 ODR-8/Ufm1 specific protease 2 promotes GPCR maturation by a Ufm1-independent
732 mechanism. *PLoS Genet* 2014, **10**(3)**:** e1004082.

733

734 42. Cai Y, Pi W, Sivaprakasam S, Zhu X, Zhang M, Chen J*, et al.* UFBP1, a Key Component
735 of the Ufm1 Conjugation System, Is Essential for Ufmylation-Mediated Regulation of
736 Erythroid Development. *PLoS Genet* 2015, **11**(11)**:** e1005643.

737

738 43. Wu J, Lei G, Mei M, Tang Y, Li H. A novel C53/LZAP-interacting protein regulates
739 stability of C53/LZAP and DDRGK domain-containing Protein 1 (DDRGK1) and
740 modulates NF-kappaB signaling. *J Biol Chem* 2010, **285**(20)**:** 15126-15136.

741

742 44. Jiang Y, Cheng Z, Mandon EC, Gilmore R. An interaction between the SRP receptor and
743 the translocon is critical during cotranslational protein translocation. *J Cell Biol* 2008,
744 **180**(6)**:** 1149-1161.

745

746 45. Song W, Raden D, Mandon EC, Gilmore R. Role of Sec61alpha in the regulated transfer
747 of the ribosome-nascent chain complex from the signal recognition particle to the
748 translocation channel. *Cell* 2000, **100**(3)**:** 333-343.

749

750 46. Mason N, Ciufo LF, Brown JD. Elongation arrest is a physiologically important function of
751 signal recognition particle. *Embo j* 2000, **19**(15)**:** 4164-4174.

752

753 47. Walter P, Blobel G. Translocation of proteins across the endoplasmic reticulum III.
754 Signal recognition protein (SRP) causes signal sequence-dependent and site-specific
755 arrest of chain elongation that is released by microsomal membranes. *J Cell Biol* 1981,
756 **91**(2 Pt 1)**:** 557-561.

757

758 48. Walczak CP, Leto DE, Zhang L, Riepe C, Muller RY, DaRosa PA*, et al.* Ribosomal
759 protein RPL26 is the principal target of UFMylation. *Proc Natl Acad Sci U S A* 2019,
760 **116**(4)**:** 1299-1308.

761

762 49. Wang L, Xu Y, Rogers H, Saidi L, Noguchi CT, Li H*, et al.* UFMylation of RPL26 links
763 translocation-associated quality control to endoplasmic reticulum protein homeostasis.
764 *Cell Res* 2020, **30**(1)**:** 5-20.

765

766 50. García-Suárez O, García B, Fernández-Vega I, Astudillo A, Quirós LM. Neuroendocrine
767 tumors show altered expression of chondroitin sulfate, glypican 1, glypican 5, and
768 syndecan 2 depending on their differentiation grade. *Front Oncol* 2014, **4:** 15.

769

770 51. Boztug K, Järvinen PM, Salzer E, Racek T, Mönch S, Garncarz W*, et al.* JAGN1
771 deficiency causes aberrant myeloid cell homeostasis and congenital neutropenia. *Nat*
772 *Genet* 2014, **46**(9)**:** 1021-1027.

773

774 52. Hwang S, Kim S, Kim K, Yeom J, Park S, Kim I. Euchromatin histone methyltransferase
775 II (EHMT2) regulates the expression of ras-related GTP binding C (RRAGC) protein.
776 *BMB Rep* 2020, **53**(11)**:** 576-581.

777

778 53. Xu L, Gao X, Yang P, Sang W, Jiao J, Niu M*, et al.* EHMT2 inhibitor BIX-01294 induces
779 endoplasmic reticulum stress mediated apoptosis and autophagy in diffuse large B-cell
780 lymphoma cells. *J Cancer* 2021, **12**(4)**:** 1011-1022.

781

782 54. Sheard MA, Asgharzadeh S, Liu Y, Lin TY, Wu HW, Ji L*, et al.* Membrane-bound TRAIL
783 supplements natural killer cell cytotoxicity against neuroblastoma cells. *J Immunother*
784 2013, **36**(5)**:** 319-329.

785

786 55. Mirandola P, Ponti C, Gobbi G, Sponzilli I, Vaccarezza M, Cocco L*, et al.* Activated
787 human NK and CD8+ T cells express both TNF-related apoptosis-inducing ligand
788 (TRAIL) and TRAIL receptors but are resistant to TRAIL-mediated cytotoxicity. *Blood*
789 2004, **104**(8)**:** 2418-2424.

790

791 56. Chen JJ, Knudsen S, Mazin W, Dahlgaard J, Zhang B. A 71-gene signature of TRAIL
792 sensitivity in cancer cells. *Mol Cancer Ther* 2012, **11**(1)**:** 34-44.

793

794 57. Sullivan GP, O'Connor H, Henry CM, Davidovich P, Clancy DM, Albert ML*, et al.* TRAIL
795 Receptors Serve as Stress-Associated Molecular Patterns to Promote ER-Stress-
796 Induced Inflammation. *Developmental Cell* 2020, **52**(6)**:** 714-730.e715.

797

798 58. Dufour F, Rattier T, Constantinescu AA, Zischler L, Morle A, Ben Mabrouk H*, et al.*
799 TRAIL receptor gene editing unveils TRAIL-R1 as a master player of apoptosis induced
800 by TRAIL and ER stress. *Oncotarget* 2017, **8**(6)**:** 9974-9985.

801

802 59. Lu M, Lawrence DA, Marsters S, Acosta-Alvear D, Kimmig P, Mendez AS*, et al.*
803 Opposing unfolded-protein-response signals converge on death receptor 5 to control
804 apoptosis. *Science* 2014, **345**(6192)**:** 98-101.

805

806 60. Iurlaro R, Puschel F, Leon-Annicchiarico CL, O'Connor H, Martin SJ, Palou-Gramon D*,*
807 *et al.* Glucose Deprivation Induces ATF4-Mediated Apoptosis through TRAIL Death
808 Receptors. *Mol Cell Biol* 2017, **37**(10).

809

810 61. van Raam BJ, Lacina T, Lindemann RK, Reiling JH. Secretory stressors induce
811 intracellular death receptor accumulation to control apoptosis. *Cell Death Dis* 2017,
812 **8**(10)**:** e3069.

813

814 62. Lam M, Marsters SA, Ashkenazi A, Walter P. Misfolded proteins bind and activate death
815 receptor 5 to trigger apoptosis during unresolved endoplasmic reticulum stress. *Elife*
816 2020, **9**.

817

818 63. Ramkumar P, Abarientos AB, Tian R, Seyler M, Leong JT, Chen M*, et al.* CRISPR-
819 based screens uncover determinants of immunotherapy response in multiple myeloma.
820 *Blood Adv* 2020, **4**(13)**:** 2899-2911.

821

822 64. De Leo A, Chen HS, Hu CC, Lieberman PM. Deregulation of KSHV latency conformation
823 by ER-stress and caspase-dependent RAD21-cleavage. *PLoS Pathog* 2017, **13**(8)**:**
824 e1006596.

825

826 65. Johnston BP, Pringle ES, McCormick C. KSHV activates unfolded protein response
827 sensors but suppresses downstream transcriptional responses to support lytic
828 replication. *PLoS Pathog* 2019, **15**(12)**:** e1008185.

829

830 66. Azfer A, Niu J, Rogers LM, Adamski FM, Kolattukudy PE. Activation of endoplasmic
831 reticulum stress response during the development of ischemic heart disease. *Am J*
832 *Physiol Heart Circ Physiol* 2006, **291**(3)**:** H1411-1420.

833

834 67. Zhang Y, Zhang M, Wu J, Lei G, Li H. Transcriptional regulation of the Ufm1 conjugation
835 system in response to disturbance of the endoplasmic reticulum homeostasis and
836 inhibition of vesicle trafficking. *PLoS One* 2012, **7**(11)**:** e48587.

837

838 68. Liu J, Wang Y, Song L, Zeng L, Yi W, Liu T*, et al.* A critical role of DDRGK1 in
839 endoplasmic reticulum homoeostasis via regulation of IRE1α stability. *Nature*
840 *Communications* 2017, **8**(1)**:** 14186.

841

842 69. Hu X, Pang Q, Shen Q, Liu H, He J, Wang J*, et al.* Ubiquitin-fold modifier 1 inhibits
843 apoptosis by suppressing the endoplasmic reticulum stress response in Raw264.7 cells.
844 *Int J Mol Med* 2014, **33**(6)**:** 1539-1546.

845

846 70. Tsherniak A, Vazquez F, Montgomery PG, Weir BA, Kryukov G, Cowley GS*, et al.*
847 Defining a Cancer Dependency Map. *Cell* 2017, **170**(3)**:** 564-576.e516.

848

849 71. Zhu H, Bhatt B, Sivaprakasam S, Cai Y, Liu S, Kodeboyina SK*, et al.* Ufbp1 promotes
850 plasma cell development and ER expansion by modulating distinct branches of UPR.
851 *Nature Communications* 2019, **10**(1)**:** 1084.

852

853 72. Hagelkruys A, Wirnsberger G, Stadlmann J, Wohner M, Horrer M, Vilagos B*, et al.* A
854 crucial role for Jagunal homolog 1 in humoral immunity and antibody glycosylation in
855 mice and humans. *J Exp Med* 2021, **218**(1).

856

857 73. Nosak C, Silva PN, Sollazzo P, Moon KM, Odisho T, Foster LJ*, et al.* Jagn1 Is Induced
858 in Response to ER Stress and Regulates Proinsulin Biosynthesis. *PLoS One* 2016,
859 **11**(2)**:** e0149177.

860

861 74. Charnaux N, Brule S, Hamon M, Chaigneau T, Saffar L, Prost C*, et al.* Syndecan-4 is a
862 signaling molecule for stromal cell-derived factor-1 (SDF-1)/ CXCL12. *Febs j* 2005,
863 **272**(8)**:** 1937-1951.

864

865 75. Farzan M, Babcock GJ, Vasilieva N, Wright PL, Kiprilov E, Mirzabekov T*, et al.* The Role
866 of Post-translational Modifications of the CXCR4 Amino Terminus in Stromal-derived
867 Factor 1α Association and HIV-1 Entry*. *Journal of Biological Chemistry* 2002, **277**(33)**:**
868 29484-29489.

869

870 76. Kremer KN, Peterson KL, Schneider PA, Meng XW, Dai H, Hess AD*, et al.* CXCR4
871 chemokine receptor signaling induces apoptosis in acute myeloid leukemia cells via
872 regulation of the Bcl-2 family members Bcl-XL, Noxa, and Bak. *J Biol Chem* 2013,
873 **288**(32)**:** 22899-22914.

874

875 77. Pham H, Kearns NA, Maehr R. Transcriptional Regulation with CRISPR/Cas9 Effectors
876 in Mammalian Cells. *Methods Mol Biol* 2016, **1358:** 43-57.

877

878 78. Manzano M, Gunther T, Ju H, Nicholas J, Bartom ET, Grundhoff A*, et al.* Kaposi's
879 Sarcoma-Associated Herpesvirus Drives a Super-Enhancer-Mediated Survival Gene
880 Expression Program in Primary Effusion Lymphoma. *mBio* 2020, **11**(4).

881

882 79. Pelossof R, Fairchild L, Huang CH, Widmer C, Sreedharan VT, Sinha N*, et al.* Prediction
883 of potent shRNAs with a sequential classification algorithm. *Nat Biotechnol* 2017, **35**(4)**:**
884 350-353.

885

886 80. Bogerd HP, Whisnant AW, Kennedy EM, Flores O, Cullen BR. Derivation and
887 characterization of Dicer- and microRNA-deficient human cells. *Rna* 2014, **20**(6)**:** 923-
888 937.

81. Martin M. CUTADAPT removes adapter sequences from high-throughput sequencing reads. *EMBnetjournal* 2011, **17**.

82. Langmead B, Trapnell C, Pop M, Salzberg SL. Ultrafast and memory-efficient alignment of short DNA sequences to the human genome. *Genome Biology* 2009, **10**(3)**:** R25.

83. Li W, Xu H, Xiao T, Cong L, Love MI, Zhang F*, et al.* MAGeCK enables robust identification of essential genes from genome-scale CRISPR/Cas9 knockout screens. *Genome Biol* 2014, **15**(12)**:** 554.

84. Cock PJA, Antao T, Chang JT, Chapman BA, Cox CJ, Dalke A*, et al.* Biopython: freely available Python tools for computational molecular biology and bioinformatics. *Bioinformatics* 2009, **25**(11)**:** 1422-1423.

85. Clement K, Rees H, Canver MC, Gehrke JM, Farouni R, Hsu JY*, et al.* CRISPResso2 provides accurate and rapid genome editing sequence analysis. *Nature Biotechnology* 2019, **37**(3)**:** 224-226.

86. Virtanen P, Gommers R, Oliphant TE, Haberland M, Reddy T, Cournapeau D*, et al.* Author Correction: SciPy 1.0: fundamental algorithms for scientific computing in Python. *Nature Methods* 2020, **17**(3)**:** 352-352.

87. Waskom M. seaborn: statistical data visualization. *JOSS* 2021, **6**(60)**:** 3021.

913

914 88. Zhou F, Shimoda M, Olney L, Lyu Y, Tran K, Jiang G*, et al.* Oncolytic Reactivation of

915 KSHV as a Therapeutic Approach for Primary Effusion Lymphoma. *Mol Cancer Ther*

916 2017, **16**(11)**:** 2627-2638.

917

918

919 **Figures and Figure Legends**

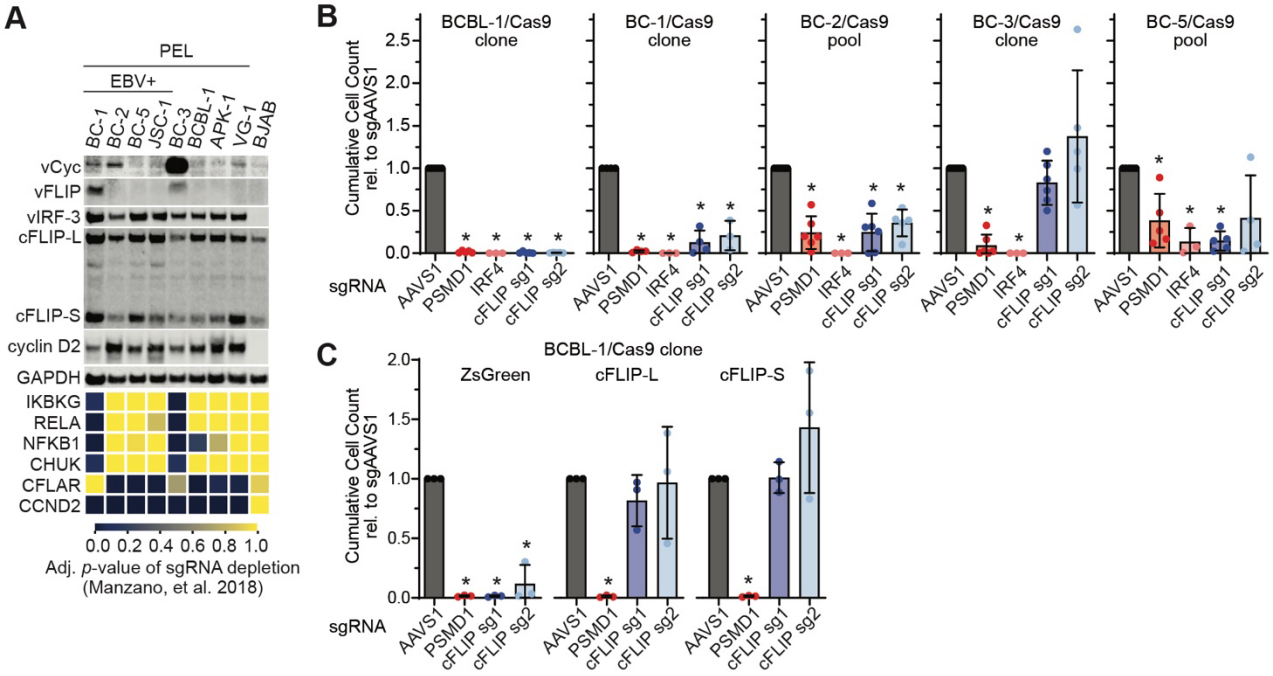

920

921 **Fig. 1** cFLIP is broadly essential in PEL cell lines. **A.** Top: Cell lysates from the indicated PEL
922 cell lines or KSHV-negative BJAB cells were analyzed by Western blotting for the indicated
923 proteins. The cFLIP splice variants cFLIP-L and cFLIP-S are marked. Bottom: Heatmap of
924 depletion for sgRNAs targeting the indicated genes, using data from Manzano, et al. 2018.
925 Lower FDR-adjusted *p*-values of depletion indicate significant sgRNA depletion in the screens,
926 suggesting essential of fitness roles. **B.** Cas9-expressing PEL cell lines were transduced with
927 the indicated sgRNAs at equal MOI 3 and selected with puromycin. Graphs show the endpoints
928 (day 8-10) of cumulative cell growth curves relative to an sgRNA targeting the safe harbor locus
929 AAVS1 (see Material and Methods). sgRNAs targeting PSMD1 and IRF4 are controls for other
930 essential genes. Error bars represent SD (n = 4-6 independent repeats). For Western Blot
931 control, see Fig. S1C. **C.** BCBL-1/Cas9 expressing ZsGreen, sgRNA-resistant cFLIP-L, or
932 sgRNA-resistant cFLIP-S were challenged with the indicated sgRNAs. Error bars represent SD
933 (n = 3 independent repeats). For Western Blot control, see Fig. S1E. In panels B and C,
934 statistical significance for loss of cell viability compared to sgAAVS1 was analyzed using one-
935 sided, one-sample t-testing (* <= 0.05). Rescue in panel C was significant as determined using
936 a one-sided, independent two-sample t-test. *p* values are listed in Table S6.

937

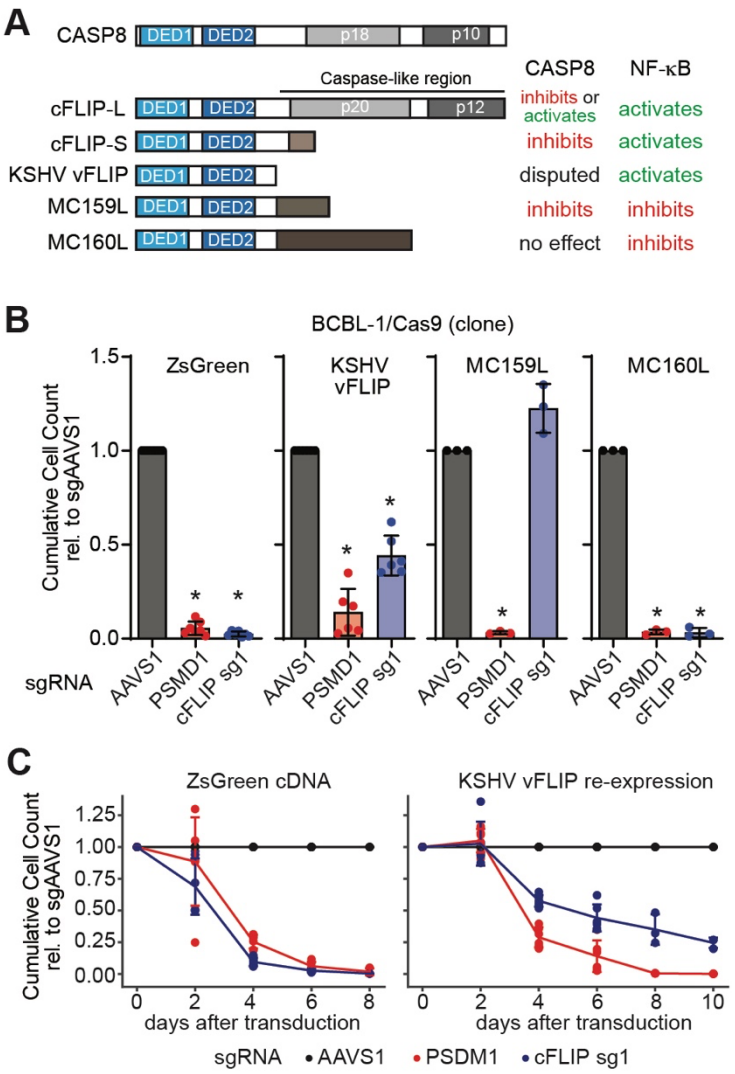

Fig. 2 cFLIP and KSHV vFLIP are functionally distinct in PEL cell lines. **A.** Schematic representation of human CASP8, the cFLIP-L/S splice variants, KSHV vFLIP, and the MCV FLIP proteins MC159L and MC160L. Also shown are the characterized activities of each protein towards CASP8/the extrinsic apoptosis pathway and the NF-κB pathway. **B.** BCBL-1/Cas9 expressing ZsGreen, KSHV vFLIP, MCV MC159L, or MCV MC160L were challenged with the indicated sgRNAs. Analyses of cumulative growth curve experiments on day 6 after sgRNA transduction are shown. Error bars represent SD (n = 3 independent repeats). For Western Blot controls, see Fig. S2. Statistical significance for loss of cell viability compared to sgAAVS1 was analyzed using one-sided, one-sample t-testing (* <= 0.05). Rescue by expression of KSHV vFLIP and MCL159L was significant as determined using a one-sided, independent two-sample t-test. *p* values are listed in Table S6. **C.** Extended growth curves for the ZsGreen and KSHV vFLIP data in panel B show that vFLIP rescue is significant, but not efficient. For details on statistical analysis see Table S6 and Material and Methods section.

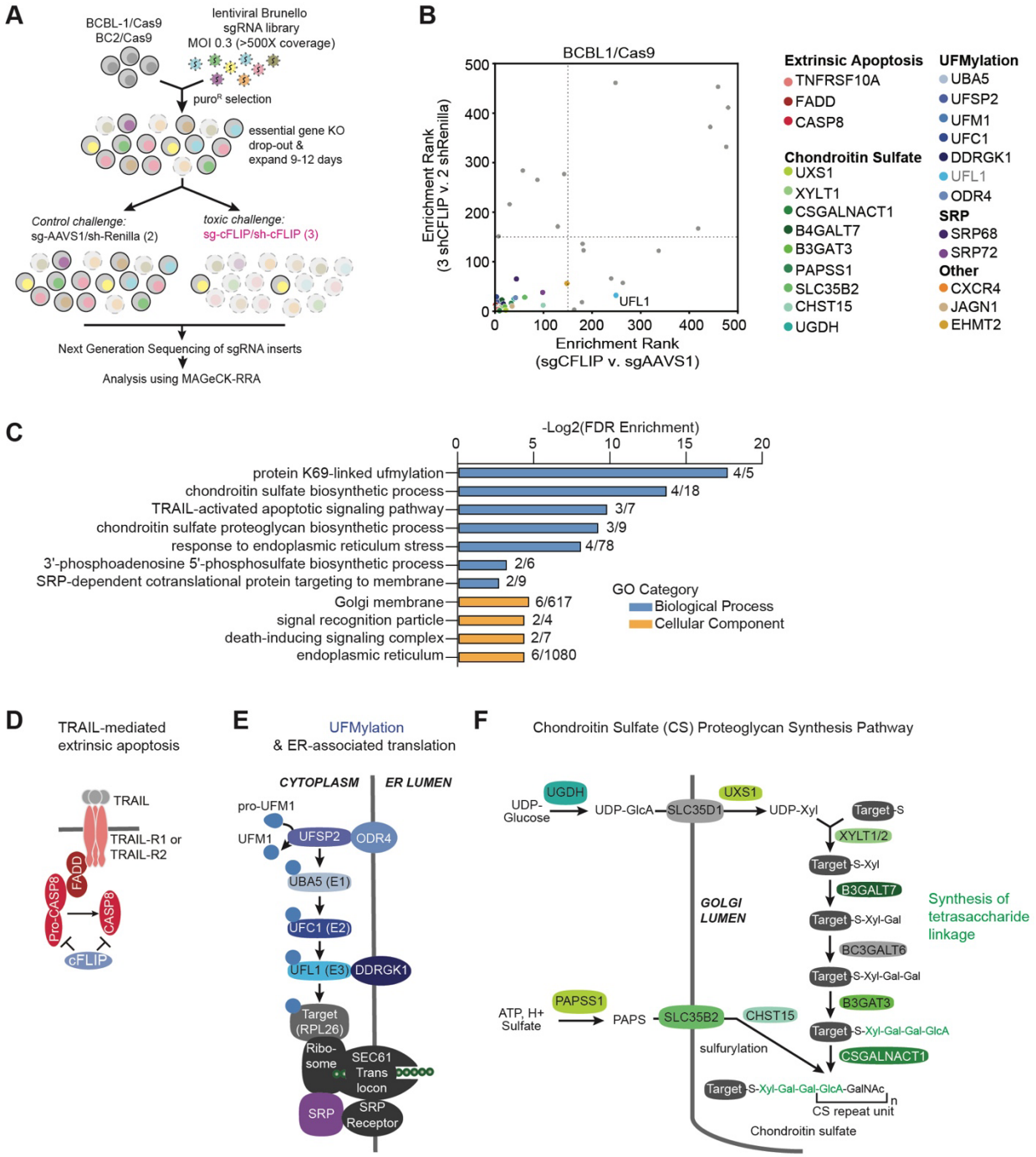

951

952 **Fig. 3.** Genome-wide synthetic rescue screens uncover components of the death program
953 repressed by cFLIP in PEL cells. **A.** Experimental design for CRISPR-based synthetic rescue
954 screening. **B.** Results of the BCBL-1 resistance screens. Shown are the gene-level ranks output
955 by MAGeCK-RRA based on library sgRNA enrichment after the toxic cFLIP shRNA challenge
956 (y-axis) or the toxic cFLIP sgRNA-challenge (x-axis) relative to matched negative control

957 perturbations. For clarity, only the top 500 hits in each screen are displayed. UFL1 was
958 highlighted as a UFMylation pathway gene but does not pass our analysis cutoff. **C.** DAVID
959 pathway analysis of the 23 high confidence hits obtained by intersecting the top 150 hits each
960 from the BCBL-1 sgRNA and shRNA screens. Numbers at right show number of hits from each
961 pathway. For complete DAVID output, see Table S3. **D.** Diagram of canonical death signaling
962 via TRAIL through TRAIL receptors. Hits are colored as in panel B. **E.** Diagram of the
963 UFMylation and ER-associated translation pathways, screening hits are colored as in panel B.
964 UFM1 is cytoplasmic, but the UFM1 conjugation machinery is anchored on the cytoplasmic face
965 of the ER membrane by adaptors ODR4 and DDRGK1 (UFBP1). RPL26 is the main
966 characterized substrate for UFMylation and impacts translational pausing during ERAD. The
967 SRP complex is involved in protein translocation and initiates translational pausing. **F.** Diagram
968 of the Condroitin sulfate (CS) proteoglycan synthesis pathway, screen hits are colored as in
969 panel B.

970

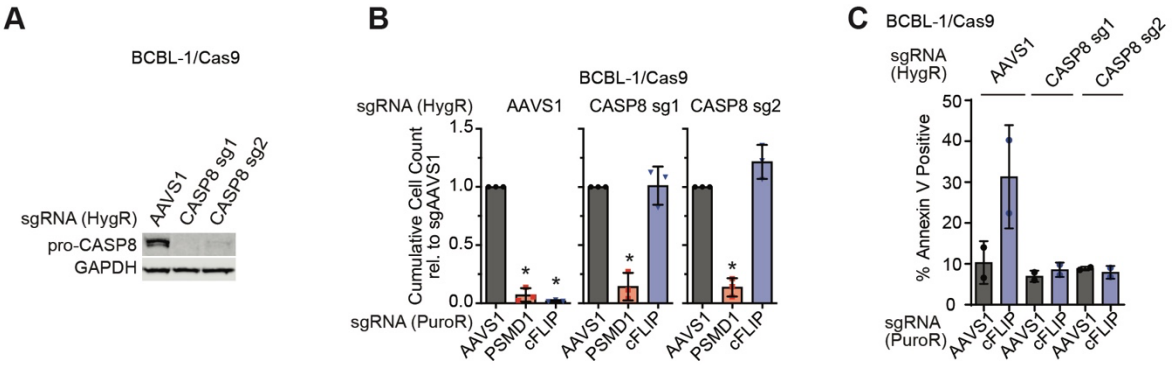

Fig. 4 Cellular FLIP protects PEL cells from CASP8-induced cell death. **A.** BCBL-1/Cas9 cells were transduced with the indicated sgRNAs, selected with hygromycin, and knockout of CASP8 was confirmed by Western blot. **B.** The cell lines from panel A were challenged with puromycin resistant lentiviral sgRNA vectors at equal MOI and cumulative growth curve analyses were performed as previously. Error bars represent SD from 3 independent repeats. For Western Blot controls, see Fig. S4D. Statistical significance for loss of cell viability compared to sgAAVS1 was analyzed using one-sided, one-sample t-testing (* <= 0.05). Rescue by CASP8 KO was significant as determined using a one-sided, independent two-sample t-test. *p* values are listed in Table S6. **C.** Cells were challenged with control or cFLIP sgRNAs as in panel B, but not selected with puromycin, and stained with Annexin V 48 hours after transduction (n=2 independent repeats, error bars indicate range).

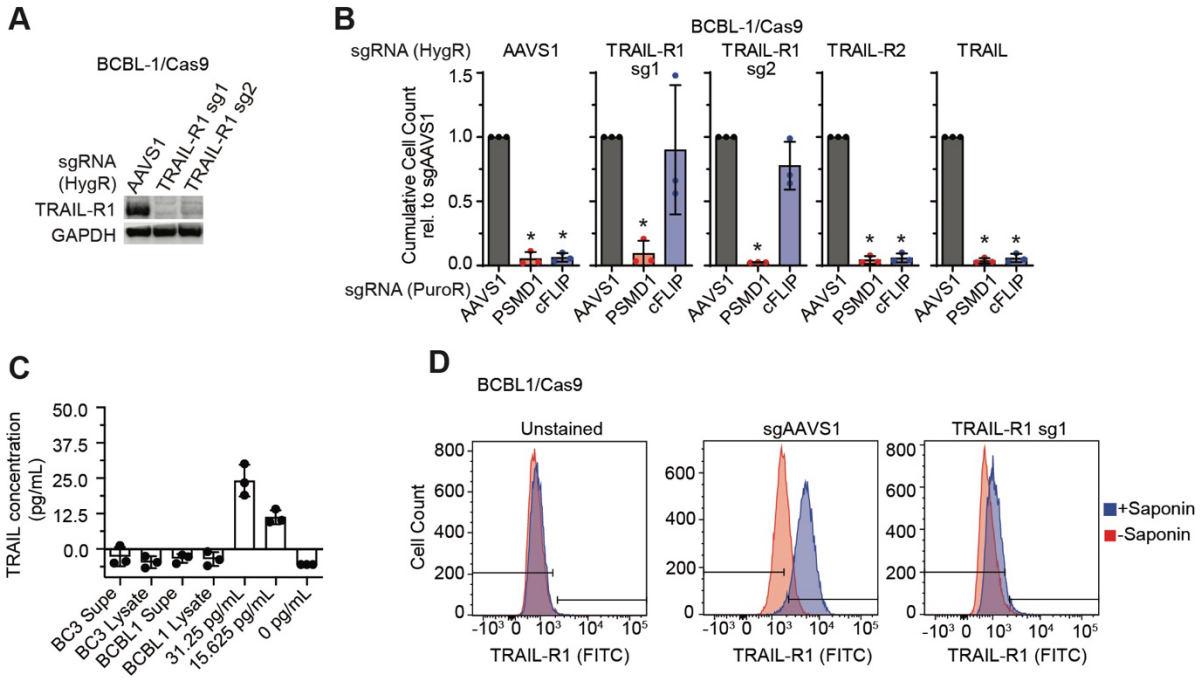

Fig. 5. Cellular FLIP protects PEL cells from a ligand-independent TRAIL-R1-mediated cell death program. **A.** BCBL-1/Cas9 cells were transduced with the indicated sgRNAs, selected with hygromycin, and knockout of TRAIL-R1 was confirmed by Western blot. **B.** Cell lines depicted in panel A were challenged with puromycin resistant lentiviral sgRNA vectors at equal MOI and cumulative growth curve analyses were performed as previously. Error bars represent SD from 3 independent repeats. For Western Blot control, see Fig. S5A. Statistical significance for loss of cell viability compared to sgAAVS1 was analyzed using one-sided, one-sample t-testing (* denotes p<= 0.05). Rescue by TRAIL-R1 KO, but not TRIAL-R2 or TRAIL KO, was significant as determined using one-sided, independent two-sample t-tests. *p* values are listed in Table S6. **C.** BC-3 or BCBL-1 cells were plated at $2x10^5$ cells/mL, and supernatants or lysates were harvested 3 days later and used for anti-TRAIL ELISA assay. Known concentrations of recombinant human TRAIL confirm sensitivity down to the ~10 pg/mL range. **D.** Knockout cell lines were fixed in 4% PFA and stained for TRAIL-R1 with or without permeabilization by saponin. Shown at left are unstained control cells. Quantification over 3 independent repeats can be found in Fig. S6C.

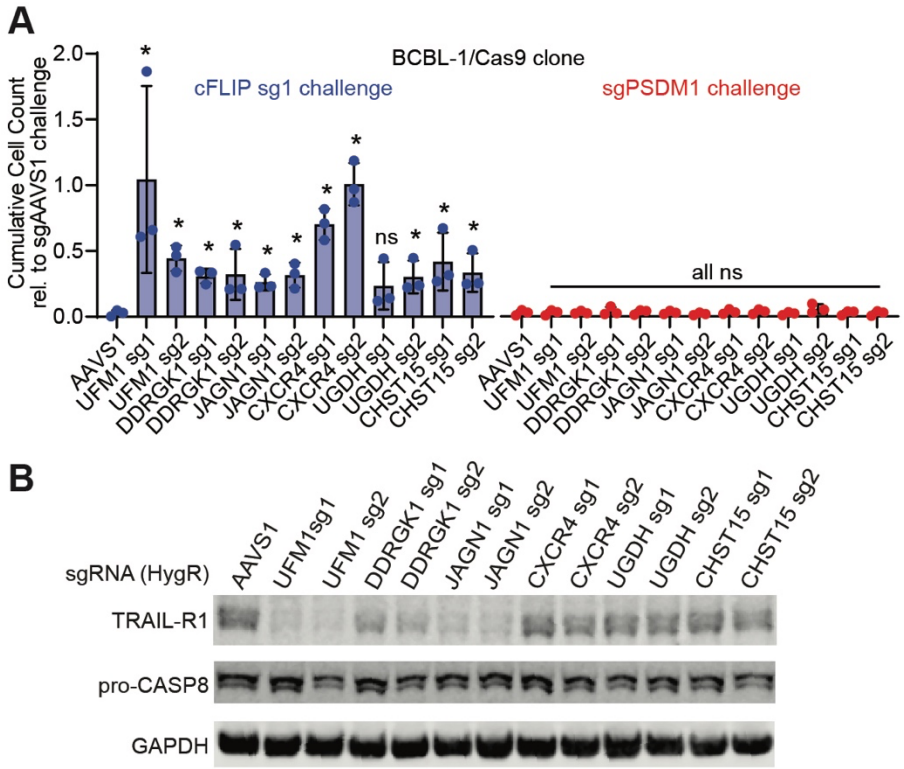

Figure 6. Knockdown of genes that participate in UFMylation, the chondroitin sulfate synthesis pathway, or of JAGN1 and CXCR4 overcome cFLIP dependency in PEL cells. **A.** Single-gene knockout pools were generated as previously for two genes each in the UFMylation and chondroitin sulfate biosynthesis pathway along with CXCR4 and JAGN1 and these cell lines were used to perform cumulative growth curves following transduction with a second sgRNA as previously. Statistical significance of rescue from sg-cFLIP induced cell death was determined using one-sided, independent two-sample t-tests (* denotes p<= 0.05). *p* values and statistical significance of loss of viability are listed in Table S6. Western controls are in Fig. S6B. **B.** Single-gene KO pools were analyzed for TRAIL-R1 and pro-caspase 8 expression by Western blotting.